Journal of Materials Chemistry A

Accepted Manuscript

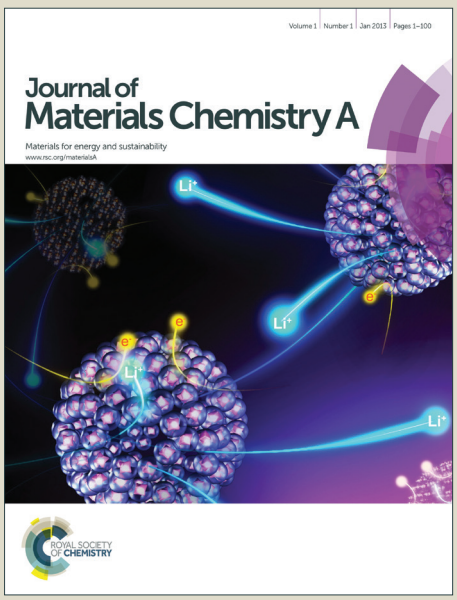

ROYAL SOCIETY OF CHEMISTRY

www.rsc.org/materialsA

Journal of Materials Chemistry A

Cite this: DOI: 10.1039/c0xx00000x

www.rsc.org/xxxxxx

PAPER

Slightly hydrogenated TiO_2 with enhanced photocatalytic performance

Yong Yan,[a+] Moyan Han,[b+] Alexander Konkin,[c] Tristan Koppe,[d] Dong Wang,[a*] Teresa Andreu,[e*] Ge Chen,[b*] Ulrich Vetter,[d] Joan Ramón Morante,[e] Peter Schaaf[a]

Received (in XXX, XXX) Xth XXXXXXXXX 201X, Accepted Xth XXXXXXXXX 201X

DOI: 10.1039/b000000x

Hydrogenated TiO_2 (H-TiO_2) has triggered intense research interests in photocatalysis due to its substantially improved solar absorption and superior activity. However, the main factors that induce the enhanced photocatalytic performance of H-TiO_2 are still under debate. In order to clarify this issue, the structural properties of H-TiO_2, and their effects on the photo-generated charges are comprehensively investigated in this study. H-TiO_2 with different hydrogenation degrees are rapidly synthesized through H_2 plasma treatment in several minutes; and their photocatalytic activity are evaluated by methylene blue (MB) degradation and CO_2 reduction in aqueous and gaseous media, respectively. The slightly hydrogenated TiO_2 (s-H-TiO_2) with the original white color exhibit the enhanced photoactivity compared with the pristine TiO_2 (pristine-TiO_2) especially in CO_2 reduction; while the gray or black H-TiO_2 with higher hydrogenation degrees (h-H-TiO_2) display much worse catalytic performances. Further investigations reveal that the higher ratio of trapped holes (O^- centers) and lower recombination rate induced by the increasing of surface defects might be the critical factors for the high activity of s-H-TiO_2; on the contrary, h-H-TiO_2 possess high concentration of bulk defects, leading to the significantly decreased amount of O^- centers and enhanced non-radiative recombination, which strongly inhibit their photoactivity. These results might provide new insights into the photoactivity of H-TiO_2, and pave the way for further studies of other hydrogenated metal oxides for photocatalytic applications.

1. Introduction

With the current threat of the exhaustion of fossil fuels and the continuing deterioration of the global environment, solar-driven catalytic process has attracted much attention, since it provide a promising "green chemistry" approach for treating a wide variety of emerging pollutants, H_2 production from water, or direct conversion of CO_2 to value-added fuels (CO, CH_4, CH_3OH, etc.).[1-3] In principle, fabrication of high active photocatalysts which can efficiently utilizing solar energy is a major challenge.[4] Titania (TiO_2) is regarded as a suitable photocatalyst due to its favorable band-edge positions, high chemical inertness, low cost, and long-term stability.[5] However, the efficiency of TiO_2 is limited due to its large band-gap and fast electron-hole recombination.[6] Hence, many studies have been devoted to overcome such problems through different approaches, which include doping with metal or nonmetal elements,[7, 8] controlling the structure and facets,[9, 10] and introducing defects into nanocrystals.[11]

Recently, hydrogenation treatment of TiO_2 has triggered intense research interests. In this process, hydrogenerated TiO_2 (H-TiO_2) with a highly disordered surface layer and a large amount of oxygen vacancies is obtained, which leads to a substantially improved optical absorption in the visible light and near-infrared region.[12-17] Therefore, H-TiO_2 usually shows a gray or black color, and exhibits superior activity for the photocatalytic degradation of organic contaminants and water splitting.[12, 15, 16, 18-22] Photo-electrochemical analysis reveal that the enhanced photoactivity of H-TiO_2 is mainly due to the improved incident photon to current conversion efficiency (IPCE) in the UV region.[15, 23] It is believed that the formation of Ti-H and Ti-O-H bonds on the surface of H-TiO_2 nanoparticles improve the separation of photo-generated electrons and holes;[12, 18, 24, 25] and the presence of Ti^{3+} species or oxygen vacancies increase the donor density of H-TiO_2, thus, facilitate the charge transportation in these nanoparticles.[15, 23, 26] On the other hand, a significantly worse photoactivity of H-TiO_2 has also been reported, and it is proposed that the poor photocatalytic performances might be ascribed to the formation of bulk defects with high temperature hydrogenation treatment.[27] In addition, the concentration of defects, and their distribution between the surface and bulk of nanocrystals is found to play an important role in enhancing the photoactivity of H-TiO_2.[28]

Despited these achievements, several problems need to be addressed for the further understanding the enhanced photoactivity of H-TiO_2: First, the properties of photo-generated electrons and holes in H-TiO_2 have not been investigated, which

have distinct dependence on its photocatalytic performance. Second, it still remains unclear whether the large solar absorption (gray or black color) of H-TiO_2 induced by disordered surface layer or high concentration of defects is really the critical factor for its excellent photocatalytic performance. Third, with the different hydrogenation methods, the structure of the obtained H-TiO_2 usually have many differences, hence, a clear assessment of the key factors in the enhanced photoactivity of H-TiO_2 by comparing these samples is not easy to achieve.

In this paper, H-TiO_2 with different hydrogenation degrees are rapidly synthesized through H_2 plasma treatment at 150 °C; and their photocatalytic activity are evaluated by methylene blue (MB) degradation and CO_2 reduction in aqueous and gaseous media, respectively. The slightly hydrogenated TiO_2 with the original white color (s-H-TiO_2) have the increased UV absorption and surface defects, and exhibit enhanced photoactivity compared to pristine TiO_2 (pristine-TiO_2) especially in CO_2 reduction. In contrast, the gray or black H-TiO_2 with higher hydrogenation degrees (h-H-TiO_2) have the highly improved visible light absorption, disordered surface layer, and a large amount of bulk defects, display much worse catalytic performances. Further investigations reveal that the increased surface defects of s-H-TiO_2 lead to the higher ratio of trapped holes (O^- centers) and lower recombination rate, which might be the critical factors for its improved photoactivity; while the high concentration of bulk defects in h-H-TiO_2 act as charge annihilation centers, most of photo-generated holes are consumed through significantly enhanced non-radiative recombination, which strongly inhibit the activity of h-H-TiO_2. These results might provide new insights into the photoactivity of H-TiO_2, and pave the way for further studies of other hydrogenated metal oxides for photocatalytic applications.

2. Experimental section

2.1 Materials and synthesis

Commercial TiO_2 nanoparticles (Degussa P25) were purchased from Sigma-Aldrich Co. and used as precursor without purification. 0.10 g TiO_2 nanoparticles were dispersed in 50 mL ethanol with an ultrasonic condition for 10 min, and then drop-casted onto a 6-inch Si wafer. The drop casting process was repeated several times to achieve a TiO_2 mass loading of 0.5 ~ 0.6 mg/cm^2 (100 ~ 150 mg on whole wafer). Then, this wafer was transferred into a chamber for plasma-enhanced hydrogenation treatment, and there an instrument of inductively coupled plasma (Plasmalab 100 ICP-CVD, Oxford Instruments) was used. The H_2 plasma treatment was performed at 150 °C for 30 s, 1 min, 3 min, 5 min, 20 min in the synthesis of H-TiO_2-30s, H-TiO_2-1min, H-TiO_2-3min, H-TiO_2-5min, and H-TiO_2-20min, respectively. The ICP power was 3000 W, the chamber pressure was 25.8~27.1 mTorr, and the H_2 flow rate was 50 sccm. After this treatment, H-TiO_2 was obtained and scratched from Si wafer for further investigations.

2.2 Photocatalytic methylene blue (MB) degradation

The photocatalytic activities of the samples in aqueous media were tested by investigating degradation of methylene blue (MB) at room temperature. The each sample containing 10 mg of TiO_2 was suspended in 40 mL MB solution (0.03 mM), and the suspension was placed into a closed container. In each experiment, the container was kept in the dark for 0.5 h to achieve adsorption and desorption equilibra with stirring. About 9.1%, 7.7%, 7.4%, 8.3%, 7.1%, and 5.4% of MB was adsorbed by pristine-TiO_2, H-TiO_2-30s, -1min, -3min, -5min, and -20min, respectively. Subsequently, solution were irradiated using 300 W Xe-lamp (full-spectrum, PLS-SXE300CUV, Perfect light, China), and at given time intervals (every 2 min), 2 mL of the suspension was collected and centrifuged (12000 r/min for 20 min) to obtain the clarify solution of dye. Then, the residual concentration of MB was measured by UV-vis absorption analysis. The peak absorbance of MB (at 666 nm) was used to determine its concentration. In the control experiment without TiO_2 catalyst, less than 5% of MB was degradated under full-spectrum irradiation for 30 min.

2.3 Photocatalytic CO_2 reduction

The photocatalytic activities of the samples in gaseous media were tested by investigating CO_2 reduction at room temperature. Each sample (90 mg) was dispersed in water and deposited over three glass substrates (conventional glass slides used for optical microscopy). The total area covered is around 60 cm^2. Evaporated at room temperature overnight, and further dried at 100 °C. Then, the samples were introduced in a stainless steel reactor with an internal volume of around 200 mL, provided with an optical window made of Borofloat 33 glass. The chamber was purged during 1 h with humid CO_2 (CO_2 bubbled though water) at a flux of 200 mL/min. Then, the valves were closed, and it was illuminated during 3h. The radiation source was a 550 W Xe-lamp with a AM 1.5G filter (solar simulator ABET Technologies, SUN2000) with a uniform illuminated area of 10 x 10 cm^2, providing 100 mW cm^{-2} in the work plane measured with a thermopile detector. After this time, the amount of CO and CH_4 evolved were quantified by a MicroGC, with two consecutives analyses.

2.4 Characterization

X-ray diffraction (XRD) pattern of the samples were recorded on a SIEMENS/BRUKER D5000 X-ray diffractometer using Cu-Kα radiation at 40 kV and 40 mA, with the samples being scanned from 2θ =10° - 90° at a rate of 0.02 °s^{-1} in Bragg-Brentano geometry. Raman spectra analysis was performed with a Renishaw In-Via System utilizing a 514.5 nm incident radiation and a 50 × aperture (N.A. = 0.75), resulting in an ~ 2 μm diameter sampling cross-section. Transmission electron microscopy (TEM) images were taken using a Tecnai F20 microscope on powder samples deposited onto a copper microgrid coated with carbon at an accelerating voltage of 200 kV. The optical absorption in the range from UV to the visible wavelength was measured by a diffuse reflectance accessory of a UV-Vis spectrometer (Cary 5000 UV-Vis-NIR). The X-ray photoelectron spectroscopy (XPS) analysis was performed by a spectrometer (Kratos Axis Ultra XPS) with monochromatized Al-Kα radiation and an energy resolution of 0.48 eV. Electron paramagnetic resonance (EPR) spectra were recorded at the temperature of 77 K using a Bruker BioSpin CW X-band (9.5 GHz) spectrometer ELEXYS E500. Light irradiation provided by two lasers (50 mW power) operated at 405nm and 532 nm using an optical transmission resonator (ER 4104OR, Bruker BioSpin).

The nanocrystals were charged in quartz glass tubes connected to N_2 gas. The hyperfine structure (hfs) lines (m_I=-3/2, -1/2, 1/2, 3/2) of the $Cu^{2+}(DTC)_2$ complex ("$Cu^{2+}L_2$" in Figure S6) in benzene solution have been used for the correct g factors of studied paramagnetic centre determination (low field maximum amplitude of m_I=-1/2 hfs line attributed to g=2.025). In the following text, the different spectra were presented as: "EPR spectra" (spectra recorded without light irradiation), "light-excited EPR spectra" (spectra recorded under irradiation) "light-induced EPR spectra" ("light-excited EPR spectra" - "EPR spectra"). Time resolved photoluminescence (PL) spectroscopy were measured by a universal streak camera (Hamamatsu C10910 using a slow single sweep unit M10913) in combination with a Czerny–Turner spectrograph (Princeton Instruments Acton SP2300, focal length 300 mm) at room temperature. Steady-state PL spectroscopy was performed by a Czerny–Turner spectrograph (Jobin Yvon SPEX 1000M) with a focal length of 1000 mm. The excitation wavelength of 266 nm was generated by a femtosecond laser (Coherent MIRA 900-F) followed by a puls picker (Coherent Pulse Picker) and a 3rd harmonic generator (APE HarmoniXX THG).

3. Results and Discussions

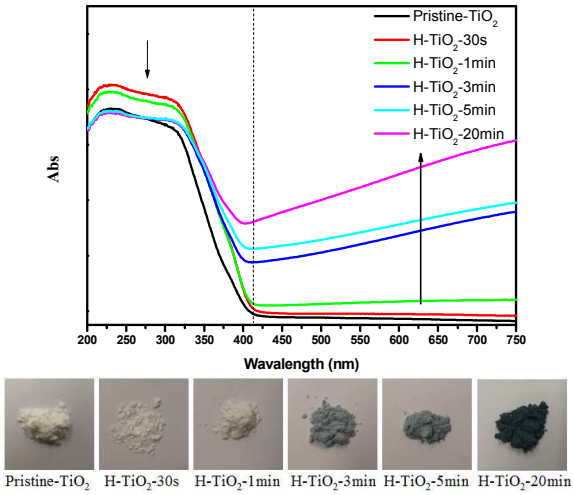

Figure 1. UV-vis absorption spectra and related photographs of the pristine-TiO_2 and H-TiO_2 prepared by H_2 plasma treatment after different times of 30 s, 1 min, 3 min, 5 min, and 20 min. (Pristine-TiO_2 represented as pristine TiO_2; H-TiO_2-30s, H-TiO_2-1min, H-TiO_2-3min, H-TiO_2-5min, and H-TiO_2-20min represented as hydrogenated TiO_2 with 30 s, 1 min, 3 min, 5 min, and 20 min H_2 plasma treatment, respectively.)

Hydrogenated TiO_2 (H-TiO_2) were obtained in a high-power density H_2 plasma treatment of purchased TiO_2 nanoparticles (Degussa P25) at 150 °C with different reaction times (the detailed parameters are given in **Experimental section**). The TiO_2 powder kept the original white color after 30 s (H-TiO_2-30s); then, TiO_2 with slightly yellow color was observed after 1 min (H-TiO_2-1min); and the color changed into gray after 3 ~ 5 min (H-TiO_2-3min and H-TiO_2-5min); with 20 min H_2 plasma treatment, black TiO_2 was obtained (H-TiO2-20min). Figure 1 shows the UV-Vis absorption spectra of pristine- and H-TiO_2. The absorption of H-TiO_2 in the region of visible light gradually increased into a high level with the extending of hydrogenation time, which clarifies the color change process from white to black. More interestingly, the slightly hydrogenated TiO_2 prepared by 30 s ~ 1 min H_2 plasma treatment (s-H-TiO_2) demonstrated an obviously improved absorption in UV region, and this improvement almost disappeared in the gray or black H-TiO_2 with higher hydrogenation degrees (h-H-TiO_2, 3 min ~ 20 min H_2 plasma treatment). It is suggested that the enhanced UV absorption might be induced by the formation of surface defects in s-H-TiO_2, the similar results has also been observed in the other materials, however, the mechanism of this phenomenon still remained unclear.[29, 30]

Figure S1 shows the XRD patterns of the pristine-TiO_2 and H-TiO_2 with different times of hydrogenation. The purchased pristine-TiO_2 nanoparticles demonstrated a major anatase phase coexisting with small amount of rutile. After H_2 plasma treatment with 30 s to 5 min, the obtained H-TiO_2 displayed almost the same XRD patterns, indicating that no phase transformation occurred in the process. However, the peak intensity of TiO_2 significantly decreased after 20 min, and the calculated average crystallite size (using Scherrer equation) of this sample in the [101] direction is 17.6 nm, which is smaller than that of pristine-TiO_2 (19.3 nm). This change might be induced by the high concentration of defects in TiO_2 nanoparticles.[15]

Figure 2 shows the HR-TEM images of pristine-TiO_2 and H-TiO_2 with different times of hydrogenation. The pristine-TiO_2 and s-H-TiO_2 were highly crystallized, as seen from the well-resolved lattice features shown in Figure 2a-c. After 3 min, a disordered layer (0.5 ~ 0.9 nm) was formed on the surface of TiO_2 nanoparticles (Figure 2d). Further prolonging the reaction time, the thickness of disordered layer increased into 1.0 ~ 1.6 and 1.5 ~ 2.2 nm after 5 and 20 min, respectively. As Raman spectra are more sensitive to disordered phase, this method was used to further investigate the structural changes of TiO_2 after different times of hydrogenation. Pristine-TiO_2 demonstrated typical anatase Raman bands at 149 cm^{-1} (E_g), 195 cm^{-1} (E_g), 397 cm^{-1} (B_{1g}), 516 cm^{-1} (A_{1g} + B_{1g}), and 638 cm^{-1} (E_g).[31] s-H-TiO_2 showed the similar patterns as pristine-TiO_2; and the peak intensity of H-TiO_2 obviously decreased upon hydrogenation time up to 3 min; after 20 min, H-TiO_2 had only a broad peak at 149 cm^{-1} with the disappearance of the other peaks, which were the characteristics of the existence of disordered phase (Figure 3).[32, 33] These results are consistent with the observation in HR-TEM images.

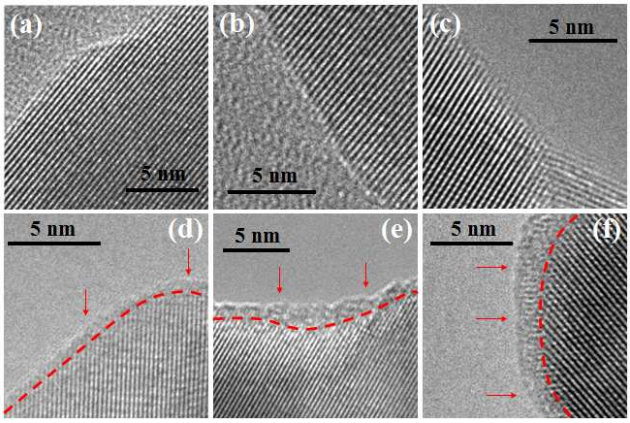

Figure 2. HR-TEM images of the pristine-TiO_2 and H-TiO_2 prepared by H_2 plasma treatment after different times: (a) Pristine-TiO_2; (b) H-TiO_2-30s; (c) H-TiO_2-1min; (d) H-TiO_2-3min; (e) H-TiO_2-5min; (f) H-TiO_2-20min.

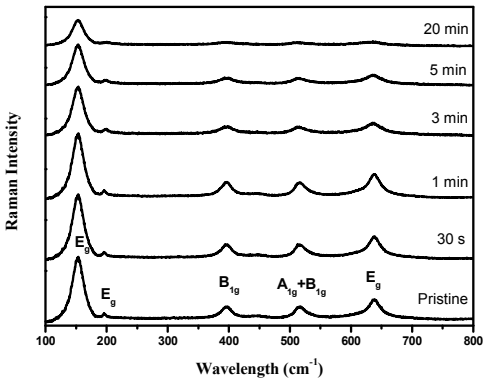

Figure 3. Raman spectra of the pristine-TiO_2 and H-TiO_2 prepared by H_2 plasma treatment after different times of 30 s, 1 min, 3 min, 5 min, and 20 min.

XPS analysis was used to investigate the changes of surface chemical bondings of the TiO_2 nanoparticles induced by hydrogenation. The Ti 2*p* core level spectrum of pristine-TiO_2 showed two peaks at ~ 458.6 and ~ 464.7 eV, corresponding to the Ti $2p_{1/2}$ and Ti $2p_{3/2}$ peaks of Ti^{4+} species;[12, 34] for H-TiO_2-30s, these peaks negative shifted to ~ 458.3 and ~ 464.5 eV, indicating a different bonding environment (upper panel in Figure 4a). Subtracting the Ti 2*p* spectrum of pristine-TiO_2 from that of H-TiO_2-30s, two extra peaks were observed at ~ 457.9 and ~ 463.6 eV, which can be attributed to the Ti $2p_{1/2}$ and Ti $2p_{3/2}$ peaks of Ti^{3+} species (lower panel in Figure 4a), indicating the presence of Ti^{3+} species on the surface of TiO_2 nanoparticles after 30 s of H_2 plasma treatment.[34, 35] Surprisingly, the Ti 2*p* peaks of H-TiO_2 re-shifted to higher values with the extending of hydrogenation time, and even closed to pristine-TiO_2 after 20 min (Figure 4b). By subtracting the Ti 2*p* spectrum of these H-TiO_2 with pristine-TiO_2, all obtained difference spectrums showed the Ti $2p_{1/2}$ and Ti $2p_{3/2}$ peaks of Ti^{3+} species, but the intensity of these peaks significantly decreased with increasing of hydrogenation time (Figure 4c). It is suggested that oxygen vacancies (Ti^{3+} sites) initially formed on the surface of TiO_2 nanoparticles under H_2 plasma treatment, and preferentially diffused into the bulk with further hydrogenation.[28, 36] The O 1*s* spectra are almost identical for the pristine-TiO_2 and all H-TiO_2 (Figure S2). Two oxygen features were obtained by peak-fitting of this spectrum: the intense peak located at 529.7 eV is the characteristic peak of Ti-O in anatase TiO_2; the broad peak centered at around 531.3 eV can be assigned to Ti-O-H.[37] The content of Ti-O-H signal in O 1*s* spectra remained at ~ 10.0% before and after different times of H_2 plasma treatment, implying that hydrogenation process has a negligible effect on the density of hydroxyl groups of the TiO_2 surface. The VB maxima were estimated by linear extrapolation of the peaks to the baselines, the pristine-TiO_2 and all H-TiO_2 displayed the band edge at ~ 2.4 eV (Figure S3). This result have also been observed in the other studies,[15, 31] which demonstrated that oxygen vacancies (or Ti^{3+} species) created by hydrogenation process could induce the formation of additional electronic states below the conduction band (CB) of TiO_2.[15, 17-20, 38] In this case, the gray or black color of H-TiO_2 with the substantially enhancement of visible light absorption might be attributed to the transitions from the TiO_2 VB to these additional electronic states or from these additional electronic states to the TiO_2 CB.[15]

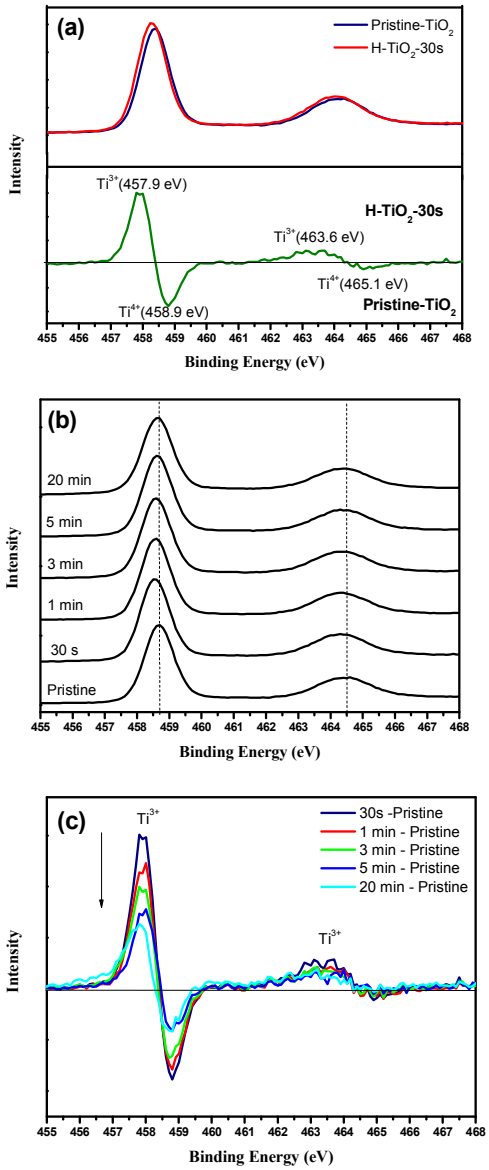

Figure 4. (a) XPS Ti 2*p* core level spectrum of the pristine-TiO_2 and H-TiO_2-30s (upper panel), and the difference spectrum obtained by subtracting the spectrum of the pristine-TiO_2 from that of the H-TiO_2-30s (lower panel). (b) XPS Ti 2*p* core level spectrum of the pristine-TiO_2 and H-TiO_2 prepared by H_2 plasma treatment after different times of 30 s, 1 min, 3 min, 5 min, and 20 min. (c) The difference spectrum obtained by subtracting the spectrum of the pristine-TiO_2 from that of H-TiO_2-30s, H-TiO_2-1min, H-TiO_2-3min, H-TiO_2-5min, and H-TiO_2-20min.

Electron paramagnetic resonance (EPR) were measured to further investigate the concentration and distribution of defects in H-TiO_2, because it is highly sensitive to detect paramagnetic species containing unpaired electrons, and has been widely used to characterize the existence of Ti^{3+} species and oxygen vacancies. As indicated in Figure 5, pristine-TiO_2 presented a weak response at a g-value of ~ 1.978, which might be ascribed to the original surface or interstitial defects in TiO_2 (Ti^{3+} species).[39, 40] After 30 s of H_2 plasma treatment, the H-TiO_2 exhibited a stronger peak with the same g-value, which indicated an increase of surface defects. After 1 min, the intensity of the surface defects signal further increased; and a broad signal at an average g-value of ~ 1.93 was also observed, which might result from the Ti^{3+} species

existed in the subsurface of TiO_2.[41, 42] After 3 min, the H-TiO_2 sample showed a much stronger signal at an average g-value of ~ 1.957 (g_x=1.965, g_y=1.960, g_z=1.945), the intensity of this signal is about 2 orders of magnitude higher than the surface Ti^{3+} species in s-H-TiO_2 (30 s ~ 1 min), implying the presence of a large amount of Ti^{3+} species in the bulk;[17, 43, 44] Prolonging the hydrogenation time to 20 min, the signal at an average g-value of ~ 1.957 with higher intensity was observed, revealing that the amount of Ti^{3+} species in the bulk further increased (~ 40 times of H-TiO_2-1min, Figure S4). These results demonstrated that the H_2 plasma treatment induced the formation of Ti^{3+} species on the surface of TiO_2 at early stage (30 s ~ 1 min), and a large amount of bulk Ti^{3+} species were formed with longer times of hydrogenation (3 ~ 20 min).

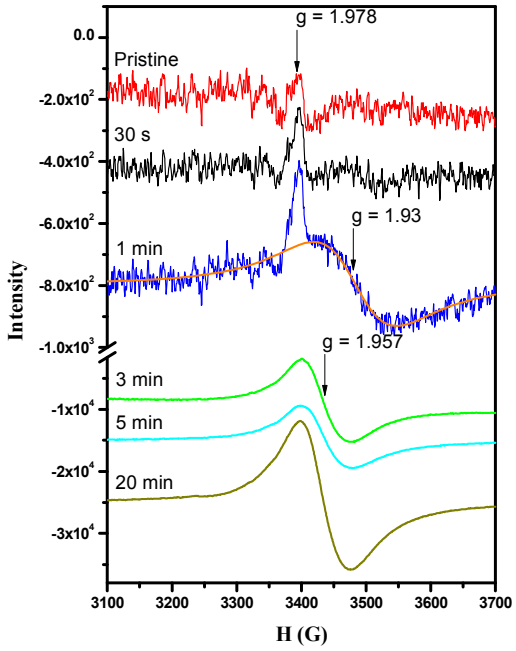

Figure 5. EPR spectra of the pristine-TiO_2 and H-TiO_2 prepared by H_2 plasma treatment after different times of 30 s, 1 min, 3 min, 5 min, and 20 min recorded at 77 K without light irradiation. (orange line presented as the simulated signal at an average g-value of 1.93)

The photocatalytic activities of H-TiO_2 were evaluated by methylene blue (MB) degradation and CO_2 reduction in aqueous and gaseous media, respectively. For MB degradation, s-H-TiO_2 exhibited better photocatalytic activities than pristine-TiO_2 (Figure 6): H-TiO_2-30s completed the decomposition of MO in 12 min; and H-TiO_2-1min needed 14 min; while the pristine-TiO_2 took 16 min. In contrast, h-H-TiO_2 showed much worse performance. About 8%, 13%, and 21% of MB remained after 16 min for H-TiO_2-3min, -5min, and -20min, respectively. The kinetics of the degradation reaction were fitted to a pseudo first-order reaction: $\ln(C_0/C)=kt$, where k is the rate constant. The average value of k for pristine-TiO_2, H-TiO_2-30s, -1min, -3min, -5min, and -20min was 0.217, 0.291, 0.255, 0.167, 0.136, and 0.101 min^{-1}, respectively (Figure S5). For CO_2 reduction, CH_4 and CO were found to be the two main products, and the similar trend as MB degradation, that the photoactivity of H-TiO_2 decreased with the increasing of hydrogenation degree, was also observed. As shown in Figure 7, s-H-TiO_2 demonstrated the enhanced conversion efficiency: the production rate of CH_4 and CO for H-TiO_2-30s was 14.65 and 19.44 $nmolh^{-1}$, respectively, which was about 2 times of pristine-TiO_2 in the total productivity (7.37 $nmolh^{-1}$ CO and 11.59 $nmolh^{-1}$ CH_4); for H-TiO_2-1min, the rate of CH_4 slightly decreased to 14.03 $nmolh^{-1}$, but the rate of CO increased to 21.67 $nmolh^{-1}$. The explanation might be that CO_2 is favourably bonded on the surface of H-TiO_2-30s due to its higher density of surface Ti^{3+} sites (Figure 4c), which enhance the immobilization of CO_2 at the surface of the catalyst, allowing a later hydrogenation to form CH_4 instead of CO.[45] For H-TiO_2-3min, the production rate of CH_4 and CO significantly decreased to 9.29 and 13.39 $nmolh^{-1}$, respectively. Nevertheless, these rates are still slightly higher than that of pristine-TiO_2, which is different with the worse performance of H-TiO_2-3min in MB degradation. This change might be induced by the different charge transfer rate in aqueous/ and gaseous/TiO_2 interface, and reaction kinetics of MB degradation and CO_2 reduction.[6] The catalytic performance of H-TiO_2 further decreased with the extending of hydrogenation time. Especially in CH_4 production, the rate is only 4.37 $nmolh^{-1}$ for H-TiO_2-5min; and almost no CH_4 signal was observed for H-TiO_2-20min. The mechanism of CO_2 photoreduction with H_2O to form CH_4 and CO can be simply described as following three steps of reaction:[45, 46]

Step 1 { Photogeneration of charges: $TiO_2 \xrightarrow{h\nu} e^- + h^+$

Step 2 { Water photooxidation : $2H_2O + 4h^+ \rightarrow O_2 + 4H^+$

Step 3 { CO_2 photoreduction to CH_4 : $CO_2 + 8H^+ + 8e^- \rightarrow CH_4 + 2H_2O$

CO_2 photoreduction to CO : $CO_2 + 2H^+ + 2e^- \rightarrow CO + 2H_2O$

According to the above mentioned results, it is suggested that the formation of high concentration of bulk Ti^{3+} is counterproductive to the photocatalytic activity of H-TiO_2. As it will be further discussed later, bulk Ti^{3+} species strongly weakened the photooxidative efficacy of h-H-TiO_2 (step 2), which reduced both the productivity as well as the selectivity CH_4/CO ratio.[45]

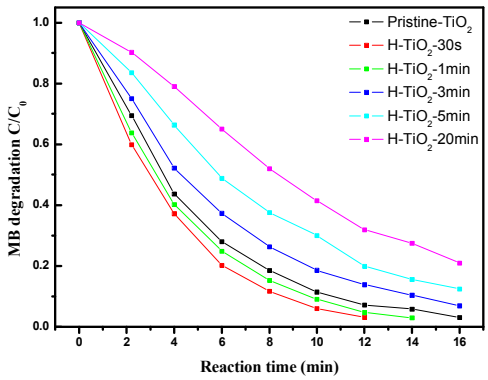

Figure 6. Degradation of methylene blue (MB) over pristine-TiO_2 and H-TiO_2 prepared by H_2 plasma treatment after different times of 30 s, 1 min, 3 min, 5 min, and 20 min. (Pristine-TiO_2, H-TiO_2-30s, H-TiO_2-1min, H-TiO_2-3min, H-TiO_2-5min, and H-TiO_2-20min)

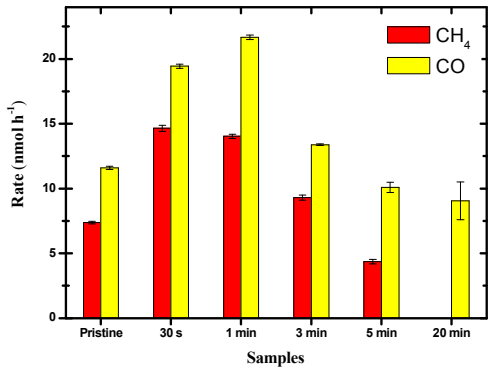

Figure 7. The formation rates of CH_4 and CO in the photocatalytic reduction of CO_2 with H_2O over pristine-TiO_2 and H-TiO_2 prepared by H_2 plasma treatment after different times of 30 s, 1 min, 3 min, 5 min, and 20 min.

In order to study the hydrogenation process affects the charge-trapping centers of TiO_2 formed upon solar light irradiation, in turn, to understand the photoactivity of H-TiO_2. Light-induced EPR measurements were performed under 405 or 532 nm light irradiation (Figure 8). For comparison, these spectrums of pristine-TiO_2 and H-TiO_2 have been subtracted by that of the spectrums without light irradiation (Figure S6). As shown in UV-vis spectra (Figure 1), the pristine-TiO_2 and s-H-TiO_2 display a steep increase in absorption at wavelengths of ~ 420 nm, hence, the irradiation with the wavelength of 405 nm can be used as excitation light source as UV light; on the other hand, the irradiation with the wavelength of 532 nm were used as visible light source. Under 405 nm light irradiation, the pristine-TiO_2 and s-H-TiO_2 showed two well-separated sets of resonance lines. The higher field small peaks with an average g value of ~ 1.960 (g_x=1.970, g_y=1.965, g_z=1.947) can be assigned to electrons trapped on Ti^{3+} centers;[39, 47] the lower field sharp features with an average g value of ~2.013 (g_x=2.022, g_y=2.015, g_z=2.003), corresponding to the holes trapped on O^- sites, [39, 47] and their intensity is greater than that of Ti^{3+} peaks. Both O^- and Ti^{3+} signals in s-H-TiO_2 showed lower intensity compared with pristine-TiO_2, indicating small part of photo-generated charges trapped by the increased surface defects.[48] After 3 ~ 5 min of H_2 plasma treatment, the intensity of O^- signals significantly decreased; and an inverted broad resonances was observed at an average g value of ~ 1.957, implying the deceasing of the amount of Ti^{3+} species in H-TiO_2, which might derive from the combination of the photo-generated holes and the localized bulk Ti^{3+} species (induced by hydrogenation). After 20 min, the O^- signals was almost disappeared, and the intensity of the inverted broad resonances further increased. This result suggested that bulk Ti^{3+} species tend to act as charge carrier traps where most of photo-generated holes were consumed through recombination with electrons.[23, 27, 40] According to the literature, the trapped holes (O^-) and electrons (Ti^{3+}) were considered as the major oxidative and reductive sites in catalytic reactions, respectively;[47] therefore, the ratio of O^-/Ti^{3+} might have an important impact on the competition between photo-oxidation and -reduction process, and thus strongly affect the efficiency of photocatalysis.[46, 47] It is observed that the ratio of O^-/Ti^{3+} is 1.71 for pristine-TiO_2 (the relative amount of Ti^{3+} and O^- can be appraised through the double integration of the resonance lines as shown in Figure S7); and this ratio increased to 2.02 and 1.84 for s-H-TiO_2 with 30 s and 1 min H_2 plasma treatment, respectively; in contrast, the ratio of O^-/Ti^{3+} dramatically decreased to less than 0.1 for h-H-TiO_2. These results indicated that s-H-TiO_2 with higher ratio of O^- centers might have enhanced photooxidative efficacy, leading to the improved photocatalytic performance; on the other hand, the worse photoactivity of h-H-TiO_2 might be attributed to the significant reduction of O^- centers, due to the formation of a large amount of bulk Ti^{3+} species with relatively long time hydrogenation. Under 532 nm light irradiation, no O^- signals were observed for the pristine- and H-TiO_2, and these samples also showed very poor visible-light photocatalytic performance in degradation of MB, revealing that the contribution of the dramatically improved visible-light absorbance of H-TiO_2 on its photoactivity is limited. This result is similar as previous reports.[15, 23]

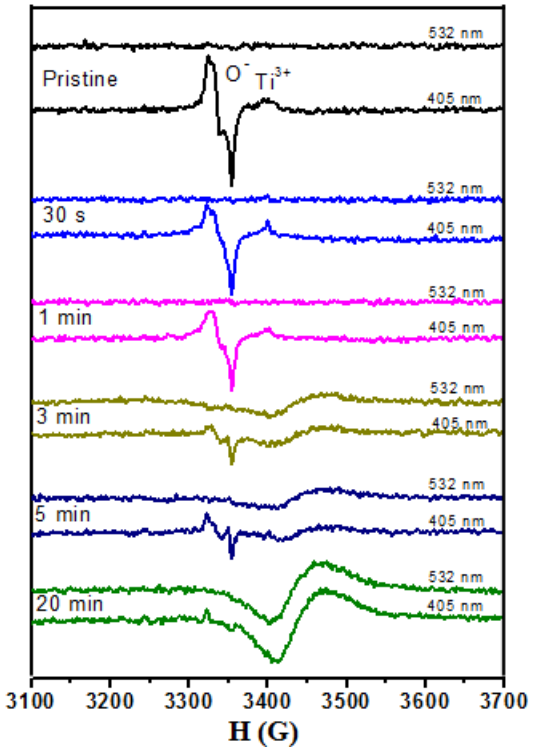

Figure 8. Light-induced EPR spectra of the pristine-TiO_2 and H-TiO_2 prepared by H_2 plasma treatment after different times of 30 s, 1 min, 3 min, 5 min, and 20 min recorded at 77 K under 405 or 532 nm light irradiation.

The photoluminescence (PL) spectra of pristine- and H-TiO_2 in the wavelength range of 420 − 680 nm with excitation at 266 nm are shown in Figure 9a. All samples exhibited a broad signal centered around 505 nm, which resulted from radiative transitions involving mobile electrons recombining with hole-trapped states (located 0.7−1.4 eV above the valence band edge), associated with oxygen vacancies in anatase TiO_2.[49, 50] H-TiO_2-30s showed a more intense and broad signal compared with pristine-TiO_2, due to its higher density of surface Ti^{3+} centers.[51] For H-TiO_2-1min, the intense of signal decreased to close to that of pristine-TiO_2, which might be induced by the existence of subsurface Ti^{3+} species. For h-H-TiO_2 (3 ~ 20 min), the signal intense significantly decreased with the increasing of hydrogenation time. This trend is consistent with the other reports, and has been considered as lower recombination rate of electrons and holes in H-TiO_2 that favors its high photocatalytic activity.[16, 18, 20, 21] Actually, in addition to radiative recombination releasing photons (detected by PL spectra), non-radiative recombination releasing phonons is a major pathway for the photo-generated charges annihilation in TiO_2 (as indirect band-

gap semiconductor). In this process, the energy is exchanged in the form of lattice vibration, and the thermal energy in materials is increased.[52, 53] Hence, the temperature changes of the pristine- and H-TiO_2 suspensions (25 mg TiO_2 in 50 mL water) were measured after 90 min of full-spectrum irradiation (Figure 9b). For pristine-TiO_2, the temperature rising was (4.5 ± 0.8) °C, which was obviously higher than that of s-H-TiO_2 ((1.2 ± 0.2) and (1.3 ± 0.2) °C for H-TiO_2-30s and H-TiO_2-1min, respectively). While the temperature rising increased to (5.7 ± 0.9), (5.9 ± 1.0), and (10.3 ± 2.2) °C for H-TiO_2 with 3, 5, and 20 min H_2 plasma treatment, respectively. These results demonstrated that s-H-TiO_2 might have lower non-radiative recombination rate compared with pristine-TiO_2 due to their limited thermal effect, but gray or black h-H-TiO_2 can more efficiently convert light energy into thermal energy, corresponding to their significantly enhanced non-radiative recombination. PL signal decay curves were used to compare the lifetime of photo-generated charges in pristine- and H-TiO_2. As shown in Figure 9c, the lifetime of electrons and holes in H-TiO_2 generally decreased with increasing of hydrogenation time. H-TiO_2-30s displayed a slightly longer lifetime than that of pristine-TiO_2, and the lifetime of H-TiO_2-1min was almost the same as pristine-TiO_2. With further hydrogenation (3 ~ 20 min), the lifetime of gray or black H-TiO_2 was shortened compared with pristine-TiO_2. Combined with light-induced EPR analysis, it is demonstrated that the surface defects in s-H-TiO_2 improve the holes trapping, and thus facilitate the separation of photo-generated charge pairs, which results in the lower recombination rate and longer lifetime of them; on the contrary, high concentration of bulk defects in h-H-TiO_2 act as charge annihilation centers, leading to the enhanced non-radiative recombination and shorter lifetime of electrons and holes.

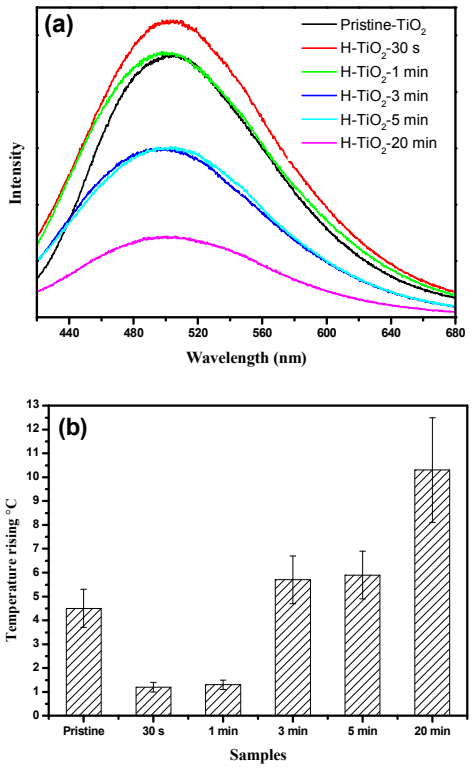

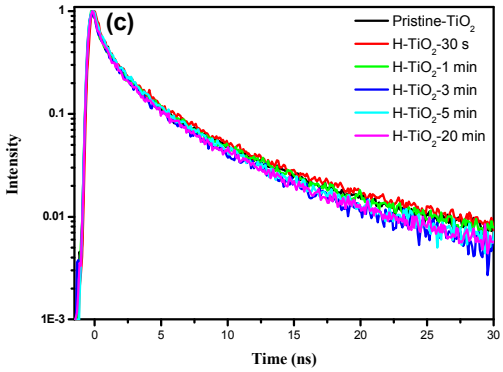

Figure 9. (a) PL spectra of the pristine-TiO_2 and H-TiO_2 prepared by H_2 plasma treatment after different times of 30 s, 1 min, 3 min, 5 min, and 20 min. (b) Temperature rising of the pristine-TiO_2, H-TiO_2-30s, H-TiO_2-1min, H-TiO_2-3min, H-TiO_2-5min, and H-TiO_2-20min suspensions (25 mg TiO_2 in 50 mL water) after 90 min of full-spectrum irradiation. (c) PL decay measured for the pristine-TiO_2 and H-TiO_2 prepared by H_2 plasma treatment after different times of 30 s, 1 min, 3 min, 5 min, and 20 min.

4. Conclusions

Hydrogenated TiO_2 (H-TiO_2) with different hydrogenation degrees are efficiently synthesized through H_2 plasma treatment in several minutes. The slightly hydrogenated TiO_2 with the original white color (s-H-TiO_2) exhibit enhanced photoactivity compared to pristine TiO_2 (pristine-TiO_2) especially in CO_2 reduction. In contrast, the gray or black H-TiO_2 with higher hydrogenation degrees (h-H-TiO_2) display much worse catalytic performances. Further investigations toward the structure and photo-generated charges of H-TiO_2 demonstrate that the improved photocatalytic performance of s-H-TiO_2 can be attributed to the higher ratio of trapped holes (O^- centers) and lower recombination rate induced by the increasing of surface defects; while the high concentration of bulk defects in h-H-TiO_2 act as charge annihilation centers, most of photo-generated holes are consumed through significantly enhanced non-radiative recombination, which strongly inhibit the activity of h-H-TiO_2.

Acknowledgement

This work was supported by the state of Thuringia (Germany) and by the European Funds for Regional Development (NanoBatt TNA VII-1/2012), National Natural Science Foundation of China (NSFC 21001012), and Beijing Nova Program (2009B06). The authors are grateful to Mr. Stefan Hanitsch from Ilmenau University of Technology for his help with sample preparation. Mr. Yong Yan is supported by means of a doctoral scholarship from the Carl Zeiss Stiftung (Germany).

Notes and references

[a] *Chair materials for Electronics, Institute of Materials Engineering and Institute of Micro- and Nanotechnologies MarcoNano®, Ilmenau University of Technology, Gustav-Kirchhoff-Str. 5, 98693 Ilmenau, Germany*
E-mail: dong.wang@tu-ilmenau.de
[b] *College of Environmental & Energy Engineering, Beijing University of Technology, Pingle yuan 100, 100124, Beijing, P.R. China*

E-mail: chenge@bjut.edu.cn
[c] *Center for Micro- and Nanotechnologies MacroNano®, TU Ilmenau, Gustav-Kirchhoff-Str. 7, 98693 Ilmenau, Germany*
[d] *II. Physikalisches Institut, Georg-August-Universität Göttingen, Friedrich-Hund-Platz 1, 37077 Göttingen, Germany*
[e] *Advanced Materials for Energy Department. Catalonia Institute for Energy Research (IREC), Jardíns de les Dones de Negre 1, Sant Adrià del Besos, Barcelona, 08930, Spain*
E-mail: tandreu@irec.cat
[+] *These authors contributed equally to this work.*
† Electronic Supplementary Information (ESI) available: Additional XRD, XPS, and EPR of pristine and hydrogenated TiO_2.
See DOI: 10.1039/b000000x/

1 M. Ni, M. K. H. Leung, D. Y. C. Leung, K. Sumathy, *Renewable Sustainable Energy Rev.* 2007, **11**, 401.
2 Y. Kuwahara, H. Yamashita, *J. Mater. Chem.* 2011, **21**, 2407.
3 S. C. Roy, O. K. Varghese, M. Paulose, C. A. Grimes, *ACS Nano* 2010, **4**, 1259.
4 A. Kudo, Y. Miseki, *Chem. Soc. Rev.* 2009, **38**, 253.
5 T. Bak, J. Nowotny, M. Rekas, C. C. Sorrell, *Int. J. Hydrogen Energy* 2002, **27**, 991.
6 A. L. Linsebigler, G. Q. Lu, J. T. Yates, *Chem. Rev.* 1995, **95**, 735.
7 A. Wang, H. Jing, *Dalton Trans.* 2014, **43**, 1011.
8 X. Chen, C. Burda, *J. Am. Chem. Soc.* 2008, **130**, 5018.
9 G. Tian, Y. Chen, W. Zhou, K. Pan, C. Tian, X. R. Huang, H. Fu, *CrystEngComm* 2011, **13**, 2994.
10 X. Han, Q. Kuang, M. Jin, Z. Xie, L. Zheng, *J. Am. Chem. Soc.* 2009, **131**, 3152.
11 M. Kong, Y. Li, X. Chen, T. Tian, P. Fang, F. Zheng, X. Zhao, *J. Am. Chem. Soc.* 2011, **133**, 16414.
12 X. Chen, L. Liu, P. Y. Yu, S. S. Mao, *Science* 2011, **331**, 746.
13 X. Chen, L. Liu, Z. Liu, M. A. Marcus, W. C. Wang, N. A. Oyler, M. E. Grass, B. Mao, P. A. Glans, P. Y. Yu, J. Guo, S. S. Mao, *Sci. Rep.* 2013, 3.
14 T. Xia, X. Chen, *J. Mater. Chem. A* 2013, **1**, 2983.
15 G. Wang, H. Wang, Y. Ling, Y. Tang, X. Yang, R. C. Fitzmorris, C. Wang, J. Z. Zhang, Y. Li, *Nano Lett.* 2011, **11**, 3026.
16 X. Jiang, Y. Zhang, J. Jiang, Y. Rong, Y. Wang, Y. Wu, C. Pan, *J. Phys. Chem. C* 2012, **116**, 22619.
17 A. Naldoni, M. Allieta, S. Santangelo, M. Marelli, F. Fabbri, S. Cappelli, C. L. Bianchi, R. Psaro, V. Dal Santo, *J. Am. Chem. Soc.* 2012, **134**, 7600.
18 Z. Wang, C. Yang, T. Lin, H. Yin, P. Chen, D. Wan, F. Xu, F. Huang, J. Lin, X. Xie, M. Jiang, *Adv. Funct. Mater.* 2013, **23**, 5444.
19 Z. Wang, C. Yang, T. Lin, H. Yin, P. Chen, D. Wan, F. Xu, F. Huang, J. Lin, X. Xie, M. Jiang, *Energy Environ. Sci.* 2013, **6**, 3007.
20 G. Zhu, T. Lin, X. Lu, W. Zhao, C. Yang, Z. Wang, H. Yin, Z. Liu, F. Huang, J. Lin, *J. Mater. Chem. A* 2013, **1**, 9650.
21 T. Lin, C. Yang, Z. Wang, H. Yin, X. Lu, F. Huang, J. Lin, X. Xie, M. Jiang, *Energy Environ. Sci.* 2014, **7**, 967.
22 Q. Kang, J. Cao, Y. Zhang, L. Liu, H. Xu, J. Ye, *J. Mater. Chem. A* 2013, **1**, 5766.
23 Y. H. Hu, *Angew. Chem. Int. Ed.* 2012, **51**, 12410.
24 W. Wei, N. Yaru, L. Chunhua, X. Zhongzi, *RSC Adv.* 2012, **2**, 8286.
25 Z. Zheng, B. Huang, J. Lu, Z. Wang, X. Qin, X. Zhang, Y. Dai, M. H. Whangbo, *Chem. Commun.* 2012, **48**, 5733.
26 X. Pan, M. Q. Yang, X. Fu, N. Zhang, Y. J. Xu, *Nanoscale* 2013, **5**, 3601.
27 T. Leshuk, R. Parviz, P. Everett, H. Krishnakumar, R. A. Varin, F. Gu, *ACS Appl. Mater. Interfaces* 2013, **5**, 1892.
28 X. Yu, B. Kim, Y. K. Kim, *ACS Catal.* 2013, **3**, 2479.
29 G. Yang, Z. Jiang, H. Shi, T. Xiao, Z. Yan, *J. Mater. Chem.* 2010, **20**, 5301.
30 Y. Sun, Z. Sun, S. Gao, H. Cheng, Q. Liu, J. Piao, T. Yao, C. Wu, S. Hu, S. Wei, Y. Xie, *Nat. Commun.* 2012, **3**, 1057.
31 Z. Lu, C. T. Yip, L. Wang, H. Huang, L. Zhou, *ChemPlusChem* 2012, **77**, 991.
32 T. Xia, W. Zhang, J. B. Murowchick, G. Liu, X. Chen, *Adv. Energy Mater.* 2013, **3**, 1516.
33 T. Xia, W. Zhang, J. Murowchick, G. Liu, X. Chen, *Nano Lett.* 2013, **13**, 5289.
34 X. Lu, G. Wang, T. Zhai, M. Yu, J. Gan, Y. Tong, Y. Li, *Nano Lett.* 2012, **12**, 1690.
35 E. McCafferty, J. P. Wightman, *Surf. Interface Anal.* 1998, **26**, 549.
36 H. Liu, H. T. Ma, X. Z. Li, W. Z. Li, M. Wu, X. H. Bao, *Chemosphere* 2003, **50**, 39.
37 G. Iucci, M. Dettin, C. Battocchio, R. Gambaretto, C. Di Bello, G. Polzonetti, *Mater. Sci. Eng. C*, 2007, **27**, 1201.
38 S. Hoang, S. P. Berglund, N. T. Hahn, A. J. Bard, C. B. Mullins, *J. Am. Chem. Soc.* 2012, **134**, 3659.
39 M. Chiesa, M. C. Paganini, S. Livraghi, E. Giamello, *Phys. Chem. Chem. Phys.* 2013, **15**, 9435.
40 L. B. Xiong, J. L. Li, B. Yang, Y. Yu, *J. Nanomater.* 2012, **2012**, 13.
41 S. J. DeCanio, J. B. Miller, J. B. Michel, C. Dybowski, *J. Phys. Chem.* 1983, **87**, 4619.
42 N. Bityurin, L. Znaidi, A. Kanaev, *Chem. Phys. Lett.* 2003, **374**, 95.
43 N. O. Gopal, H. H. Lo, S. C. Sheu, S. C. Ke, *J. Am. Chem. Soc.* 2010, **132**, 10982.
44 W. Wang, C. Lu, Y. Ni, M. Su, Z. Xu, *Appl. Catal. B-Environ* 2012, **127**, 28.
45 M. Manzanares, C. Fàbrega, J. Oriol Ossó, L. F. Vega, T. Andreu, J. R. Morante, *Appl. Catal. B-Environ* 2014, **150–151**, 57.
46 M. Tahir, N. S. Amin, *Chem. Eng. J.* 2013, **230**, 314.
47 M. D'Arienzo, J. Carbajo, A. Bahamonde, M. Crippa, S. Polizzi, R. Scotti, L. Wahba, F. Morazzoni, *J. Am. Chem. Soc.* 2011, **133**, 17652.
48 N. M. Dimitrijevic, Z. V. Saponjic, B. M. Rabatic, O. G. Poluektov, T. Rajh, *J. Phys. Chem. C* 2007, **111**, 14597.
49 N. Serpone, D. Lawless, R. Khairutdinov, *J. Phys. Chem.* 1995, **99**, 16646.
50 F. J. Knorr, C. C. Mercado, J. L. McHale, *J. Phys. Chem. C* 2008, **112**, 12786.
51 M. V. Dozzi, C. D'Andrea, B. Ohtani, G. Valentini, E. Selli, *J. Phys. Chem. C* 2013, **117**, 25586.
52 C. Hamaguchi, Basic Semiconductor Physics, Springer, Heidelberg, Germany, 2009.
53 J. Liu, J. Li, A. Sedhain, J. Lin, H. Jiang, *J. Phys. Chem. C* 2008, **112**, 17127.

Graphical abstract:

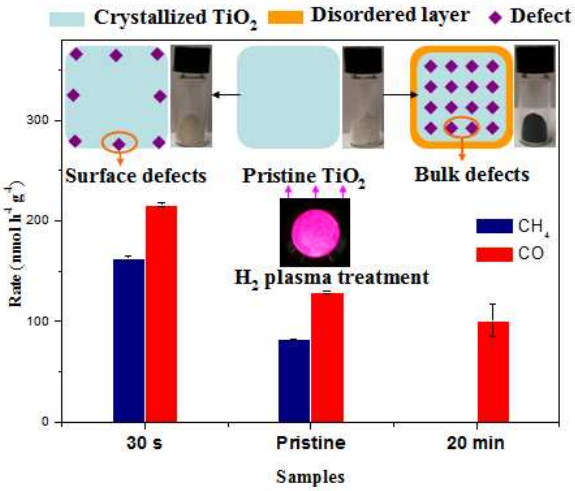

Slightly hydrogenated TiO_2 nanoparticles with original white color were efficiently synthesized through 30 s ~ 1 min H_2 plasma treatment, which showed enhanced photocatalytic performance, due to its increased surface defects. On the contrary, the gray or black H-TiO_2 with higher hydrogenation degrees display much worse catalytic performances, which can be attributed to the substantially weakened photooxidative efficacy and enhanced non-radiative recombination with the formation of bulk defects.